Research Square

Preprints are preliminary reports that have not undergone peer review.
They should not be considered conclusive, used to inform clinical practice,
or referenced by the media as validated information.

First successfully accomplished application and results on LGAD/nLGAD detector performance in laser-driven proton-boron (p-B) fusion plasma diagnostics

Miloš Manojlović

milos.manojlovic@imb-cnm.csic.es

Instituto de Microelectrónica de Barcelona

Gordana Laštovička-Medin

Faculty of Natural Sciences and Mathematics, University of Montenegro

Przemysław Tchórz

Institute of Plasma Physics & Laser Microfusion (IPPLM)

Tomáš Laštovička

ELI Beamlines Facility, The Extreme Light Infrastructure ERIC

Raj Laxmi Singh

ELI Beamlines Facility, The Extreme Light Infrastructure ERIC

David Prokop

ELI Beamlines Facility, The Extreme Light Infrastructure ERIC

Michael Ehret

ELI Beamlines Facility, The Extreme Light Infrastructure ERIC

Florent Dougados

Instituto de Microelectrónica de Barcelona

Neil Moffat

Instituto de Microelectrónica de Barcelona

Pablo Fernández-Martínez

Instituto de Microelectrónica de Barcelona

Gregor Kramberger

Jožef Stefan Institute

Enric Cabruja

Instituto de Microelectrónica de Barcelona

Salvador Hidalgo

Instituto de Microelectrónica de Barcelona

Giulio Pellegrini

Instituto de Microelectrónica de Barcelona

Article

Keywords:

Posted Date: May 14th, 2026

DOI: https://doi.org/10.21203/rs.3.rs-9556470/v1

License: This work is licensed under a Creative Commons Attribution 4.0 International License.
Read Full License

Additional Declarations: No competing interests reported.

First successfully accomplished application and results on LGAD/nLGAD detector performance in laser-driven proton-boron (p-B) fusion plasma diagnostics

Miloš Manojlović[1,*], Gordana Laštovička-Medin[2], Przemysław Tchórz[3], Tomáš Laštovička[4], Raj Laxmi Singh[4], David Prokop[4], Michael Ehret[4], Florent Dougados[1], Neil Moffat[1], Pablo Fernandez-Martínez[1], Gregor Kramberger[5], Enric Cabruja[1], Salvador Hidalgo[1], and Giulio Pellegrini[1]

[*]milos.manojlovic@imb-cnm.csic.es
[1]Instituto de Microelectrónica de Barcelona (IMB-CNM-CSIC), 08193 Cerdanyola del Valles, Barcelona, Spain
[2]Faculty of Natural Sciences and Mathematics, University of Montenegro, Džordža Vašingtona, Podgorica, 81000, Montenegro
[3]Institute of Plasma Physics & Laser Microfusion (IPPLM), Hery 23, 01-497 Warsaw, Poland
[4]ELI Beamlines Facility, The Extreme Light Infrastructure ERIC, Za Radnicí 835, Dolní Břežany, 25241, Czech Republic
[5]Jožef Stefan Institute, Jamova cesta 39, Ljubljana, 1000, Slovenia

ABSTRACT

High-intensity laser pulses used during laser-matter interaction generate intense bursts of X-rays together with energetic charged particles, whose detection is crucial during laser ion acceleration or laser-driven fusion experiments. Accurate time-of-flight (ToF) diagnostics in this environment require fast and radiation-tolerant detectors capable of operating under strong electromagnetic pulse (EMP) conditions. In this work, we investigate p-type and n-type Low Gain Avalanche Detectors (LGADs) as diagnostic tools in a proton-boron (p-B) fusion oriented, laser-driven experiment conducted at ELI-Beamlines facility using L4n laser system. For the first time, LGADs are employed in a laser fusion environment to measure time-of-flight signals, exhibiting a response consistent with an alpha-particle contribution across a wide spectrum of particle energies and emission angles. The detectors successfully resolved prompt X-ray signals and subsequent charged-particle arrivals, enabling reconstruction of an energy spectrum compatible with that of alpha particles. Post-experimental electrical characterization confirms preserved gain, and any radiation-induced damage is below the detectable level. These results not only demonstrate the feasibility of LGAD technology as a fast timing diagnostic for aneutronic fusion studies, but laser-plasma research in general.

Introduction

Over the last decade, the proton–boron (p-B) fusion reaction[1] has gained attention as a neutron-free alternative for energy production. In contrast to conventional and well-established fusion reactions such as deuterium–deuterium (D-D) or deuterium–tritium (D-T), the main products (and simultaneously energy carriers) of the p-B fusion reaction are three alpha particles, as shown in equation (1):

$$p + {}^{11}\mathrm{B} \rightarrow 3\,{}^{4}\mathrm{He}^{+} + 8.7\,\mathrm{MeV} \tag{1}$$

As a consequence, this reaction does not produce neutron-induced material activation and therefore results in much less nuclear waste production, while also offering the potential for direct conversion of fusion energy into electricity via radio-voltaic conversion rather then thermal steam production. While the p-B reaction is difficult to exploit in magnetic confinement fusion due to the significantly higher plasma temperatures required to overcome the larger Coulomb barrier, the protons inducing this reaction are readily obtainable through laser-driven ion acceleration, as the maximum of the cross-section for p-B fusion peaks at 650 keV[2] of proton kinetic energy. Consequently, the majority of research is conducted using laser systems, typically following either the pitcher–catcher or the in-plasma approach. In the pitcher–catcher scenario, two separate phases can be identified: the generation and emission of protons from a primary target (the pitcher), which subsequently irradiate a secondary boron-rich target (the catcher)[3]. In the in-plasma approach, direct laser irradiation of a target containing both hydrogen and

boron leads to the formation of a short-lived plasma in which the reaction occurs[4]. In both scenarios, prompt emission of X-rays and visible light occurs during plasma formation inside primary target (made of polyethylene or hydrogenated compounds), followed by the emission of electrons and ions. This temporal separation of ionizing radiation enables the use of time-of-flight (ToF) methods for the identification and characterization of alpha-particle bunches originating from the p-B reaction. Among a variety of methods developed for accurate measurement of alpha particles produced in this reaction[5], the detection approach based on nuclear track detectors[6] currently provides the most reliable diagnostic method for identifying alpha particles and determining their number and energy spectrum. However, their post-experiment processing and generally lengthy data analysis do not allow for real-time measurements. Therefore, the development of ToF methods, based either on novel approaches[7] or on the development of new types of detectors[8], remains an active field of research not only in laser-driven p-B fusion but also in the broader laser–plasma research community.

This paper focuses on the Low Gain Avalanche Detectors (LGAD)[9] - silicon detectors built on either p- or n-type substrate with a highly doped ($\sim 10^{16}$–$10^{17}\,\mathrm{at/cm^3}$) so-called gain layer (made out of boron or phosphorus respectively) diffused in between it's substrate and the junction implant. By introducing this doped layer, a strong electric field is established close to the detector surface, allowing internal multiplication of charge generated upon radiation incidence, increasing the output signal magnitude. Precise doping of the gain layer enables controlled charge multiplication, allowing for proportional response, distinguishing this technology from Avalanche Photodiodes (APDs)[10]. LGADs built on p-type substrate ($n^+/p^+/p/p^{++}$) are suitable for detection of high-penetrating radiation, as the avalanche in such case is primarily driven by electrons drifting back from the bulk towards the n++ electrode (electrons are the main contributors to gain, as the impact ionization coefficient for electrons is higher than for holes). On the other hand, n-type LGADs (nLGAD) ($p^+/n^+/n/n^{++}$)[11] are an application-specific technology, aiming for the detection of deep-UV, vacuum-UV and soft X-rays. In these devices, electron-driven avalanche occurs only if electrons are created prior to the gain layer, which is why they are suitable for shallow-penetrating radiation detection. P-type LGADs have evolved as a mature technology and have been tested multiple times on different types of radiation such as photons, protons, beta particles, ions etc. They have excellent timing performance of the order 20–30 ps[12], which makes them a chosen technology for the Minimum Ionizing Particle Timing Detector (MTD) for the Compact Muon Solenoid (CMS) and the High-Granularity Timing Detector (HGTD) for the A Toroidal LHC ApparatuS (ATLAS) experiment, respectively. The concept of the nLGAD has been proven[13], though the optimization of this technology is still ongoing at the Instituto de Microelectrónica de Barcelona-Centro Nacional de Microelectrónica (IMB-CNM).

In the context of this paper, considering their proven performance in High Energy Physics (HEP) application, selecting LGADs as the diagnostics in fusion experiments is justified since they have the key following properties:

- High sensitivity to charged particles due to internal gain
- Sensitivity to X-rays[14,15]
- Fast response, suitable for time-of-arrival measurements in high-dose rate experiments[16]
- High radiation hardness: capable of withstanding radiation fluence up to 3×10^{15} 1 MeV neutron equivalent ($\mathrm{neq/cm^2}$)[17]

To the best of our knowledge, this study presents the first use of LGADs in a laser-fusion related experiment and should therefore be considered a feasibility study. The following sections provide a brief overview of the experiment, describe the experimental measurements, and discuss the results.

Methods

Experimental setup

Measurements presented in this work were performed during a laser-fusion-related experiment conducted using the L4n laser system at the ELI Beamlines (Dolní Břežany, Czech Republic). During the described campaign, the system delivered laser pulses with an energy $E_L = 430\,\mathrm{J}$, a pulse duration $\tau = 1$ ns a focal spot diameter $d_F = 30$ µm and a wavelength $\lambda = 527$ nm. The main goal of the experiment was to drive D-D nuclear reactions through the so-called Cavity Pressure Acceleration mechanism[18–20]. In this mechanism, plasma generated during laser–matter interaction is confined by the geometry of the target, resulting in increased pressure, density, and temperature of the plasma plume. In addition to the possibility of driving D-D fusion reactions, an intense burst of charged particles (including protons with energies of approximately 1 MeV) is emitted from the cavity during plasma release, even in the absence of deuterated materials. This makes the method suitable for applications in p–B reactions or for performing hybrid-fusion experiments, which was one of the goals of this experimental campaign. The standard approach for ToF detectors in such experiments relies on the use of metallic filters placed in front of the detector housing in order to suppress heavy-ion contributions and reduce their influence on the recorded signal. However, as the LGAD detectors were used for the first time in a harsh mixed-radiation environment, it was crucial to ensure that the detected signal

remained uncontaminated by other radiation components. Therefore, instead of exposing the detectors to a wide range of ionizing radiation and relying on filters to prevent saturation, the use of the pitcher–catcher geometry during the p-B phase of the experiment allowed the LGAD detectors to be installed at a position where only prompt X-rays and alpha particles emitted from the irradiated side of the boron target could be detected, while simultaneously limiting the exposure to ions and electrons emitted from the primary cavity target from reaching the detector (Fig. 1). In this contribution, only several characteristic shots are analyzed in order to emphasize the potential of LGAD detectors as diagnostics in fusion-related research.

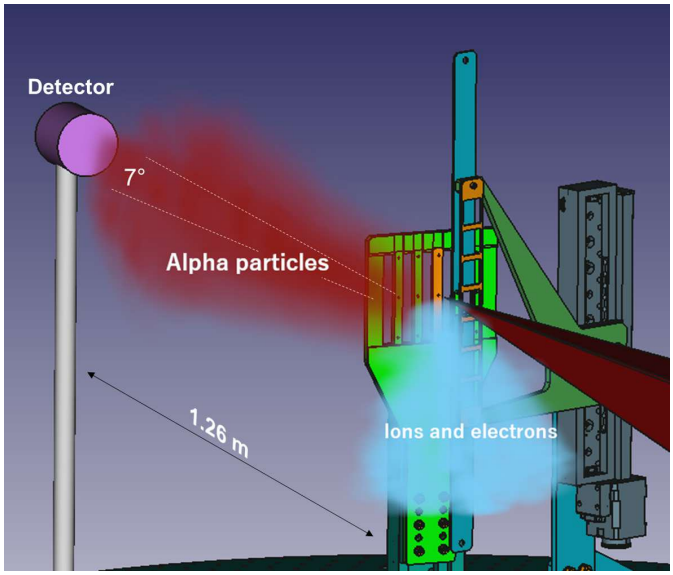


Figure 1. A schematic of the experiment is shown, illustrating the direction of laser propagation, position of LGAD detector chosen for alpha particle detection, setup of primary and secondary target and geometry of emitted charged particles.

Samples and mounting

Two different types of LGAD samples were used in this study: p-type LGADs with a deep multiplication layer (d.LGADs)[21] and standard n-type LGADs from IMB-CNM production, schematically shown in Fig. 2.

The d.LGAD sensors were produced in two splits: with carbonated and a non-carbonated gain layer. Introducing carbon into the gain layer[22] has been shown to slow down the acceptor removal mechanism, which is one of the main causes of gain degradation in LGADs under irradiation, affecting the timing resolution, rise time and time of arrival. Therefore, for this campaign, a carbonated d.LGAD was used as a device-under-test (DUT), as it is a more radiation hard design.

The structural characteristics of the two sensor types differ. The d.LGAD devices are 5 mm × 5 mm chips, with an active thickness of 55 µm, supported by a 500 µm handle substrate. The n-type LGAD samples are 3 mm × 3 mm with a thickness of 300 µm. The devices have one guard ring (GR), which was left floating during the experiment.

Regarding surface processing, nLGAD samples are fully metallized with 1.5 µm thick aluminum and covered by 0.7 µm of Si_3N_4 and 0.4 µm of SiO_2, whereas the d.LGAD devices are covered with 30 nm of titanium, a 1.5 µm aluminum layer, and are passivated the same way as nLGAD. Samples with a fully metallized surface were intentionally selected as DUTs because the metal layer attenuates the energy of the incident ions. Since the detector response depends on the ion penetration depth, a partial metallization would lead to different penetration depths of impinging ions, i. e. different responses between the center of the detector and the edges. To avoid such response variations, a fully metallized samples were used. Their main specifications are summarized in Table 1.

The detectors were mounted inside a custom aluminum housings (Fig. 3) designed to suppress electromagnetic pulse (EMP) noise. The customized housing (originally designed for TCT studies) serves as a Faraday cage, and was produced at the Jožef Stefan Institute (Ljubljana, Slovenia). These housings have passed the Residual Gas Analysis (RGA) tests, to prevent possible chemical contamination of the fusion chamber.

The housing includes a circular 2-mm aperture allowing radiation to reach the detector. The housings were installed on a metal holder equipped with a rotational stage for angular alignment with the expected particle trajectories. The detector height could also be adjusted so that the height corresponds to the height of the interaction point.

The readout chain consisted of a Bias-T (Particulars BT-01), a high-voltage supply, and a 2-GHz oscilloscope (KEYSIGHT InfiniiVision DSOX6004A 20 GSa/s). which were kept outside the chamber. The chamber was maintained at 1.8×10^{-6} mbar

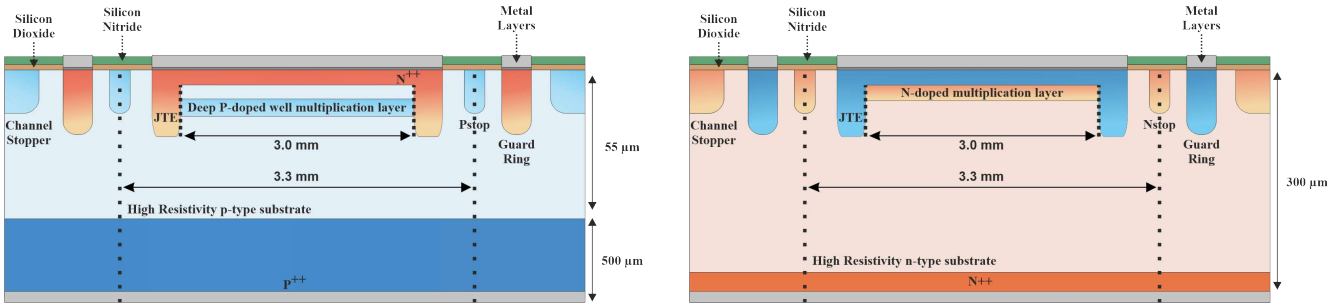


Figure 2. (a) Schematics of d.LGAD; (b) Schematics of standard nLGAD.

Parameter	d-LGAD	nLGAD
Type	Carbonated	Standard
Active Thickness	55 µm	300 µm
Substrate Thickness / Material	555 µm / p-type Si	300 µm / n-type Si
Area	5 mm × 5 mm	3 mm × 3 mm
Passivation	Si_3N_4 + SiO_2 (0.7 µm + 0.4 µm)	Si_3N_4 + SiO_2 (0.7 µm + 0.4 µm)
Metallization	Ti (30 nm) + Al (1.5 µm)	Al (1.5 µm)

Table 1. Key specifications of the samples used in the p-B experiment.

vacuum to prevent charged-particle energy loss en route to the detectors. All external electronics were wrapped in aluminum foil to further reduce the EMP. A 20-dB attenuator ensured signal amplitudes remained within the oscilloscope limits. A 50 Ω input termination was added to suppress reflections due to impedance mismatch, signal distortions and preserve the waveform shape. The experiment was triggered by the L4 laser trigger distributed by the MRF (Micro-Research Finland) timing system[23]. For the LGAD detectors, the trigger timing was calibrated against a fast Si photodetector (Thorlabs DET025A/M) placed at the Potassium dihydrogen phosphate (KDP) conversion crystal location and subsequently corrected for the optical path from the KDP crystal to the target chamber center (TCC) in the plasma physics platform (P3) chamber. This correction accounted for 11.7 m of propagation in air to the chamber window and an additional 2.4 m in vacuum inside the chamber, yielding an estimate of the laser arrival time at the TCC with ns-level precision.

EMP assessment

The impact of Electromagnetic Pulses (EMP) was successfully mitigated for measurements with LGAD detectors. This section gives a detailed discussion of EMP signatures and their dependence of the respective electronic circuits. Type RG142 coaxial cables were used for the transport of signal and bias voltage. All cables inside the interaction chamber were protected with a grounded braid, from the detector outputs to the feedthrough. Signals were recorded on a KEYSIGHT InfiniiVision DSOX6004A at 20 GSa/s, providing $\sim$ 50 ps sampling. For comparison, both LGAD detector mounted inside the chamber and a SiC detector were analyzed. The SiC detector, while not used as an active detector in this campaign, was deployed externally to monitor the EMP outside the chamber.

Chamber eigenmodes are present in data recorded with the SiC detector mounted outside the interaction chamber (Fig. 4. These eigenmodes are typically represented as TM_{mnp} (Transverse Magnetic) or TE_{mnp} (Transverse Electric) modes, while the indices m, n, and p correspond to the angular, radial, and longitudinal coordinates of the cavity, respectively. The peak at $\sim$ 48 MHz is consistent with TM_{010} of a cavity with effective radius $\sim$ 2.4 m, and a cluster of modes around 110–120 MHz is consistent with TE_{012}/TE_{121}/TM_{021} pointing to an effective height of $\sim$ 3.45 m, slightly above the nominal 3.3 m. All modes exhibit higher harmonics.

In contrast, LGAD measurements exhibit no cavity modes but two reflection combs. One with a spacing of $\sim$ 22.8 MHz, pronounced at $\{41.6, 63.2, 85.6, 106.4, 129.6, 153.6, 177.6\}$ MHz (each $\pm$5 MHz), corresponding to a round-trip delay of (43.9 ± 0.4) ns; and another with a spacing of $\sim$ 23.8 MHz, pronounced at $\{51.2, 74.4, 98.4, 122.4\}$ MHz, corresponding to a round-trip delay of (42.1 ± 0.1) ns. These round trip delays are equivalent to (4.34 ± 0.08) m and (4.17 ± 0.01) m of transmission line respectively.

Given the use of a bias-T and the $>$ 4 m supply-to-detector distance (with a short $<$ 1 m detector-to-oscilloscope cable), these combs are most consistent with cable reflections on the bias path rather than chamber cavity pickup. Note that the

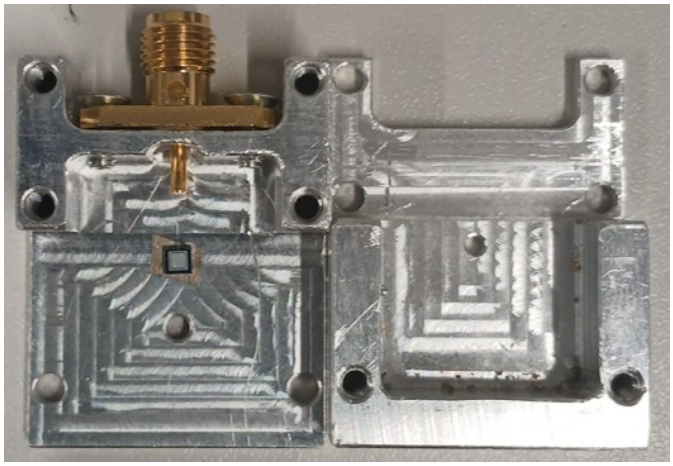


Figure 3. Aluminum housing inside of which the detectors are mounted.

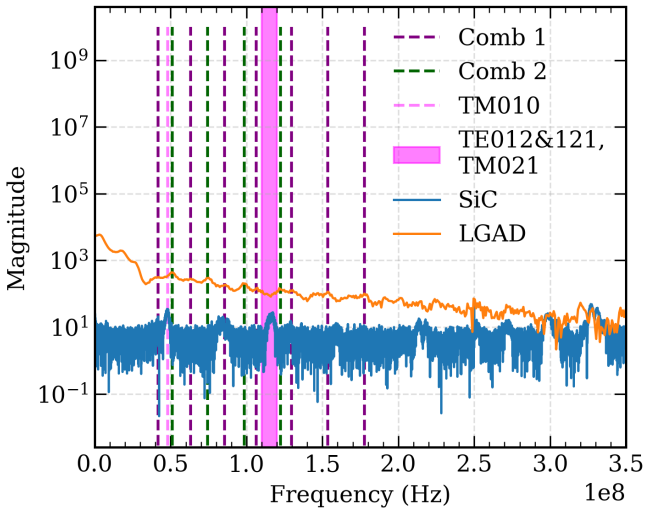


Figure 4. Typical frequency-domain magnitude spectrum of the recorded signals for two detectors, showing characteristic peaks associated with electromagnetic interference.

sampling rate of the acquisition is able to support the inferred $\sim$ 42–44 ns delays and to exclude aliasing as the root cause of the MHz-scale comb spacing. However, we do not intend to compare the performance of the LGAD directly to the SiC detector, this discussion should only illustrate the presence of strong modes. The SiC detector was mounted outside the vacuum chamber at a position which demanded longer cabling (supply-to-detector $>$ 10 m, detector-to-oscilloscope a few meters). A pick-up of EMP by the extra cable might well explain the higher sensitivity of the circuit to chamber fields.

The absence of cavity-mode signatures in LAGD detector channels indicates that the detector readout was effectively shielded from chamber EMP. This, in itself, is a valuable technical accomplishment for these ns–kJ interactions.

Results and discussion

Transient analysis

The laser driven fusion experiment is conducted in successive laser shots, with a geometry already described in the introduction. This paper does not address the side where protons/ions and electrons are generated (Fig. 1); instead, the focus is on analyzing signals from detectors positioned on the side where alpha particles are produced. The position of the LGAD diagnostics inside the fusion chamber is shown in Fig. 5. In principle, depending on the shot number, i.e., laser energy, focus and target type, different particles are generated, with emphasis that the generation depends on whether a secondary target was used or not. The space angle was chosen in such a way that when the secondary target is used, alpha particles will be registered in the detectors,

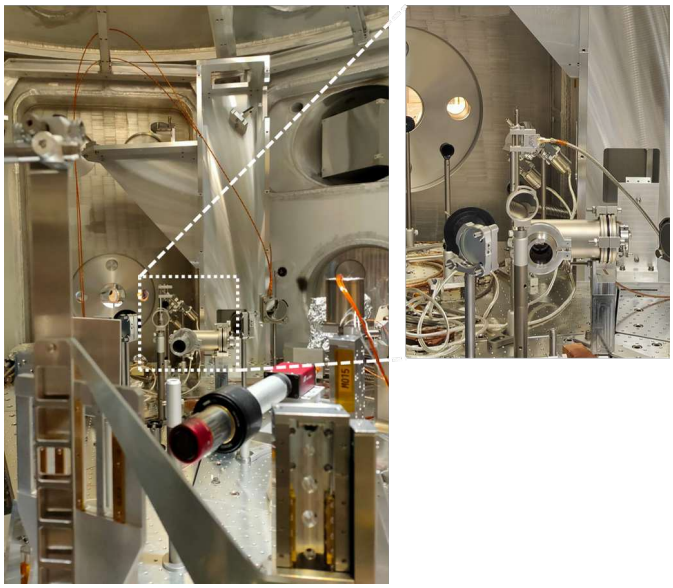


Figure 5. Position of LGAD diagnostics in the fusion chamber during the experiment.

along with an X-ray shower. However, if no secondary target is used, the signal in the LGAD/nLGAD should come mostly from photons in the soft to hard X-ray range.

Each shot takes place on the time scale of the minute, and transient is recorded for a single shot. Signals induced on the d.LGAD detector (placed in the position shown in Fig. 1), with and without secondary target introduced, are presented in Fig. 6.

The time axis is referenced to the trigger signal (t = 0). In both cases, the sharp peak related with the arrival of X rays is visible at the beginning of the signal, followed by gradual decay where specific peak-like features are present. The primary difference between the two traces is the signal amplitude, indicating that the secondary target contributes an additional particle flux while preserving the overall detector response. Subtracting the signals, one obtains a smooth, broad hump-like structure characterized by a gradual increase of the signal, a wide maximum between approximately 40 and 70 ns, and a long monotonic decay afterwards (Fig. 6, red line). The only sources of signal in this geometry could be either a broad spectrum of

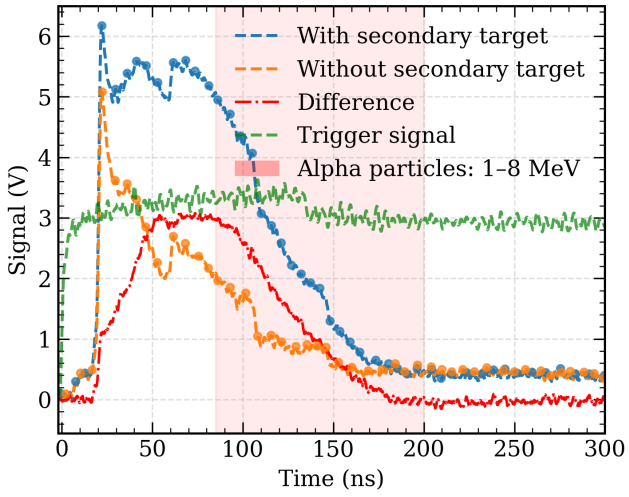


Figure 6. Signal transients in a d.LGAD detector for two configurations: with and without a secondary target. The difference between the two signals is also shown, highlighting contributions from the secondary target. The shaded region indicates the time window (85–200 ns) where signals from alpha particles in the 1–8 MeV energy range are expected. This energy range corresponds to Bragg peak positions of approximately 0.3 μm and 46 μm within the detector depth, respectively.

electromagnetic radiation produced during the initial laser–matter interaction (and subsequently during the plasma–secondary target interaction) or alpha particles originating from the p-B reaction that successfully reached the active layer of the detector. Therefore, the early part of the signal can be attributed to an additional source of electromagnetic radiation associated with the pitcher–catcher interaction. Under this assumption, the signal observed at times $t > 85$ ns can be identified as originating from alpha particles. Knowing the detector distance of 126 cm, the measured ToF can be converted into the corresponding particle energies, assuming that only alpha particles contribute to the recorded signal. The effect of such energy reconstruction is shown in Fig. 7. The broad, quasi-Maxwellian energy spectrum with a pronounced maximum near 3 MeV is consistent with the expected products of the proton–boron reaction[20], and the observed energy range agrees well with spectra typically reported in laser-driven p-B experiments[24]. According to Stopping and Range of Ions in Matter (SRIM)[25] simulation, when all these surface layers are taken into account, the penetration depth of 3 MeV alpha particles is $\sim$ 12 µm. Furthermore, for the highest-energy alpha spectrum ($\sim$ 8 MeV), the Bragg peak is located at a depth of approximately $\sim$ 46 µm.

Fig. 8 shows transients from the nLGAD when the sample is positioned at a location similar to that of the d.LGAD. Although signals were recorded for different shots involving different target configurations (primary only, or primary + secondary), it is not possible to reliably assign the origin of the peak that appears at around 110 ns (the small "kink" in the signal). In some cases, i. e., for some laser shots shown in the legend, peaks with a fast leading edge appear, originating from the X-ray bursts. However, before the charge is collected, additional ionization occurs, without any systematic relation to whether a primary or secondary target was used. The different slopes of the signal traces suggest varying contributions, likely arising from convolutions/superpositions of signals produced by different ionization processes impinging on the detector. However, based on the present measurements alone, it is not possible to unambiguously identify which specific reaction induced such a signal, since there is no clear difference between the signals obtained with the primary target only and those obtained with both primary and secondary targets. In particular, there is a shot-to-shot variation in the magnitude of the signal that likely reflects different types of particles, different entry positions, different angles of incidence, and plasma effects slowing the collection.

The observed change in the slope of the falling edge of the transients may also originate from Compton-scattered photons or electrons. A definitive identification would require correlation with additional diagnostic tools, such as a Thomson parabola[26], or other complementary measurements taken with other ToF diagnostics during the experiment. Overall, the results indicate the limitation of nLGAD in particle discrimination under these specific conditions, suggesting that improved diagnostic strategies or detector configurations should be considered for the future applications. Meanwhile, d.LGAD was successfully used to record signals interpreted as arising from alpha particles produced in the p–B reaction. Additionally, the observed difference in response between the two could be attributed to the differing bulk thicknesses, with the d.LGAD being thinner ($\sim$ 55 µm), explaining also why its collection time is shorter. In contrast, the nLGAD is much thicker ($\sim$ 300 µm), and the drift of charge carriers takes several tens of nanoseconds. In this detector, holes are collected, which are 2–3 times slower than electrons. As a result, the signal from a single particle can take $\sim$ 40 ns to be fully collected, leading to a significant superposition of pulses,

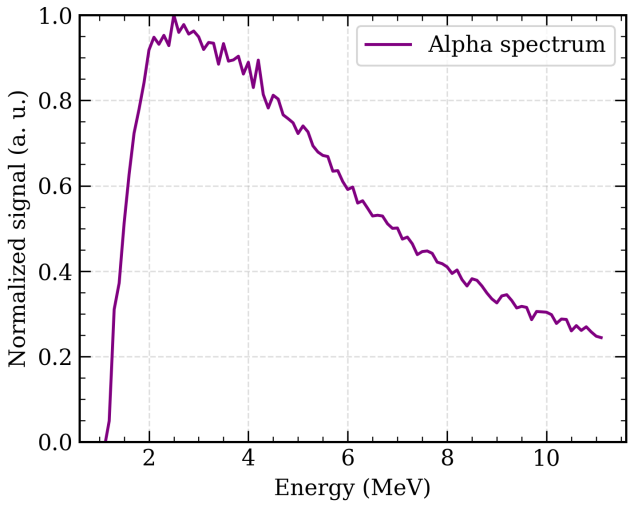


Figure 7. Indicative ToF-derived spectrum obtained under the assumption that the late-time excess signal is dominated by alpha particles. Each time coordinate t_{ns} was converted into a kinetic energy via $E = \frac{1}{2} m_\alpha (L/(t_{\mathrm{ns}} \cdot 10^{-9}))^2$, where $L = 1.26$ m is the distance from source to detector, $m_\alpha = 6.644 \times 10^{-27}$ kg is the alpha particle mass, t_{ns} is the ToF in nanoseconds, and the y-axis represents the difference signal scaled by t^3 and normalized to its maximum value.

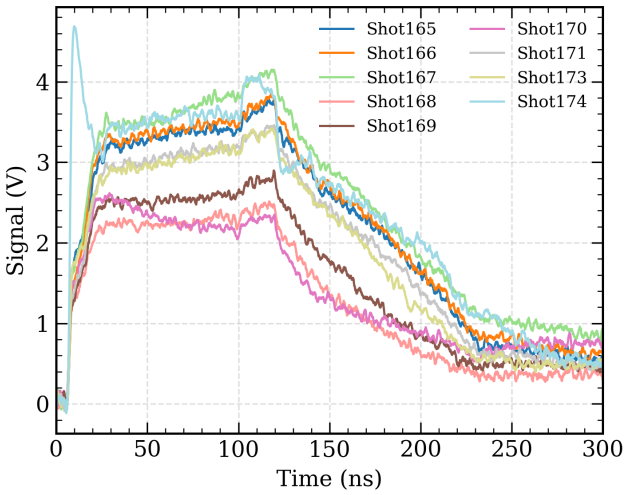


Figure 8. Signal transients induced in nLGAD across different laser shots. The first column in the legend represents signals with only the primary target, while the second column represents signals obtained when the secondary target was also used.

making deconvolution very challenging. This effect is much less pronounced for thin p-type LGADs, where electrons are collected and the drift time is short, resulting in faster and cleaner signals.

In the end, it must be pointed out that the gain response of the LGAD/nLGAD technology is strongly dependent on the density of electron–hole (e–h) pairs created inside the detector. It has been reported in ion-microprobe experiments, that the gain probed with heavy ions is always significantly and temporarily reduced, and is lower than when measured by laser, due to the so-called gain suppression (GS) mechanism[27]. The large number of e-h pairs generated by highly ionizing ions, and further multiplied within the gain layer, produces electric field screening, which in turn temporarily quenches the total gain. Multiple studies have shown that the gain of LGADs is higher when ions strike at an angle compared to normal, perpendicular incidence[28]. The GS effect is also observed with photons[29–31], provided that a sufficient laser fluence is used to probe the detector, with a strong dependence on the wavelength of the laser. In the experiment, different ionizations interact with the LGAD at various angles, having different penetration depths (Bragg peak positions), resulting in a gain response that is a superposition of multiple contributions, complicating the charge dynamics. Such plasma effect could also have impact on the ToA and the overal signal shape recorded by nLGAD. This is best illustrated by comparing the transients from shots 174 (Fig.8) with those of other shots. In the case of shot 174, a fast rise time is observed, originating from the photopeak itself, whereas the transients from other shots show a spoiled ToA. This could be an example of how gain suppression (GS) impacts timing[32]. In order to fully understand the transients attributed to alpha particles, a dedicated study using alpha-TCT should be employed. This work is, however, beyond the scope of the present paper.

During each laser shot, the leakage current was recorded in real time. The levels of leakage current in successive laser shots were increasing. After several shots, the leakage current approached the compliance limit of the HV supply, triggering an automatic voltage ramp-down and preventing reverse bias conditions, and therefore further measurements.

Fig. 9 shows the one example of the evolution of leakage current over successive exposures, compared to the virgin detector at 100 V. The leakage increases by three orders of magnitude even only after the first laser shot. This behavior is most likely induced by dynamic charging, i.e., the buildup of positive oxide charges in the surface due to X-ray burst exposures, which disappears once the surface charges redistribute. Thermal effects can be neglected, as the heat dissipated by a pulse is $E_{\text{pulse}} = I \cdot V \cdot t = \frac{5\ \text{V}}{50\ \Omega} \cdot 200\ \text{V} \cdot 200 \times 10^{-9}\ \text{s} \approx 4\,\mu\text{J}$. The effect becomes increasingly pronounced during successive laser shots, which are separated by approximately three minutes.

To confirm that the current read during the experiment is likely due to temporary effects caused by surface charges, rather than radiation induced damage, an I–V and C–V post-characterization was performed.

Post-characterization

As already mentioned in the introduction, one important issue with LGAD-based technology is the loss of gain at hadron fluences on the order of $3 \times 10^{15}\,\text{cm}^{-2}$ (1 MeV-neutron equivalent), while for ion exposures of nLGADs, even lower fluences have been reported[33,34] to degrade the gain. The effect is attributed to acceptor/donor removal mechanism[35]. The existence of gain in LGADs is easily verified by the existence of a kink in the capacitance curve, with values of around 25-29 V necessary

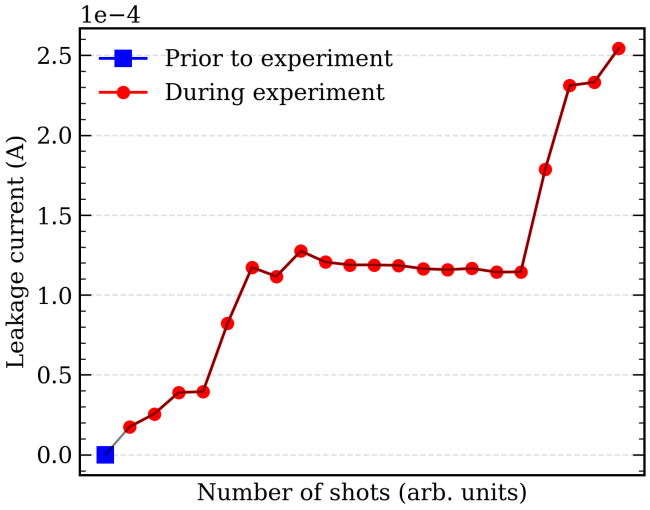


Figure 9. Leakage current evolution with successive laser shots. The first point represents the initial current prior to the experiment, while subsequent points show the increase during the experiment. The trend is consistent across all samples, regardless of substrate type.

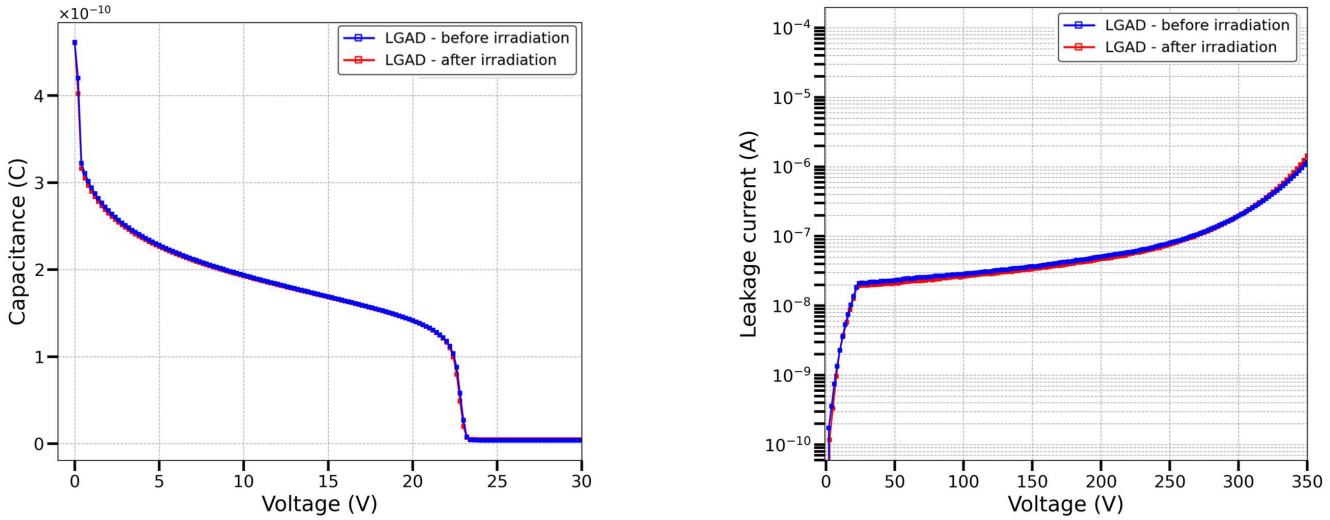


Figure 10. (a) C–V measurement on d.LGAD samples before and after experimental campaign; (b) and I–V characteristic of d.LGAD samples after the experimental campaign.

to deplete the gain (V_{gl}) layer and reach the electric field magnitudes on the order of $3-4\times10^5\,\mathrm{V/cm}$ necessary for the multiplication to occur. Higher values of V_{gl} correspond to higher gain, and vice versa. Typically, high-fluence exposure to hadrons and ions leads to a significant decrease in V_{gl}, indicating gain degradation. Therefore, measuring the C–V and extracting the V_{gl} before and after exposure is a reliable indication of the change in gain. One such measurement, performed on an LGAD sample, is shown in Fig. 10a, with no change in V_{gl} observed. In addition to this, due to radiation induced defects, leakage current of the silicon detectors usually goes up. When the I-V is measured after the experiment and compared to the virgin detectors, no change in the performance is seen. This is shown in Fig. 10b. These results suggest that LGADs remain radiation-hard under standard p-B fusion conditions.

This is understandable when the charge from the subtracted signal from Fig. 6 is integrated (starting after 65 ns), which yields $Q = 3.80\times10^{-9}$ C, corresponding to the $N_e = Q/e \approx 2.37\times10^{10}$ of electrons in silicon. On the other hand, 3 MeV alpha particle in silicon generates approximately $N_{eh} = 3\times10^6\,\mathrm{eV}/3.6\,\mathrm{eV} \approx 8.33\times10^5$ e-h. The effective number of alpha

particles is then $N_\alpha = N_e/N_{eh} \approx 2.8 \times 10^4$. These $\sim$ 28,000 alpha particles are generated over cumulative hundreds of shots. Such small number of alpha particles could explain why radiation damage is negligible.

Summary

In this work, for the first time the performance of p-type d.LGAD and n-type LGAD detectors was investigated as diagnostic tools in a laser-induced, fusion-relevant experiment. The detectors were exposed to a mixed radiation environment consisting of X-rays, laser-driven ion beams and secondary charged particles under high-EMP conditions. ToF measurements were successfully performed using the prompt X-ray emission as a temporal reference. The reconstructed detector response is consistent with an alpha-particle contribution in a p-B relevant geometry, obtained by d.LGAD detectors and lies in excellent agreement with other experimental works, whereas no systematic transients were recorded by the nLGAD, which saturates faster due to its thicker active layer, resulting in a slower decay of the falling edge. Despite the qualitative character of acquired data, this work represents the first real testing of LGAD detectors in high-density, high-EMP conditions. LGADs were used to record fast transients, but for the large signals observed, their intrinsic gain seems to offer little advantage. It would be interesting to evaluate the performance of other flavours of this technology, such as Deep Junction LGAD (DJ-LGAD) or ultra-shallow junction nLGAD (USJ-nLGAD) proposed by IMB-CNM, under conditions equivalent to those investigated in this work, to evaluate whether gain layer depth and thickness have any impact on the timing performance and signal reconstruction. Alternatively, it could be that thin p-type PiN diodes ($\sim$ 20 µm) would be a better choice, providing good time binning and easier spectrum deconvolution.

Data availability

The data that support the findings of this study is available from the corresponding author on reasonable request.

References

1. Batani, K. Perspectives on research on laser driven proton-boron fusion and applications. *J. Instrumentation* **18**, DOI: 10.1088/1748-0221/18/09/c09012 (2023).
2. Hegelich, B. M., Labun, L., Labun, O. Z. & Mehlhorn, T. A. Photon and neutron production as in situ diagnostics of proton-boron fusion. *Laser Part. Beams* **2023**, e7, DOI: 10.1155/2023/6924841 (2023).
3. Liu, A. *et al.* Enhancement of proton-boron nuclear reactions by utilizing a meshed catcher target. *Phys. Rev. Appl.* **20**, 034053, DOI: 10.1103/PhysRevApplied.20.034053 (2023).
4. Giuffrida, L. *et al.* High-current stream of energetic α particles from laser-driven proton-boron fusion. *Phys. Rev. E* **101**, 013204, DOI: 10.1103/PhysRevE.101.013204 (2020).
5. Consoli, F. *et al.* Diagnostic methodologies of laser-initiated ^{11}b(p,α)2α fusion reactions. *Front. Phys.* **8**, DOI: 10.3389/fphy.2020.561492 (2020).
6. Schollmeier, M. S. *et al.* Differentiating multi-mev, multi-ion spectra with cr-39 solid-state nuclear track detectors. *Sci. Reports* **13**, 18155, DOI: 10.1038/s41598-023-45208-x (2023).
7. Raso, A. M. *et al.* Multi-filter diamond array time-of-flight particle detector in laser–plasma experiments. *Rev. Sci. Instruments* **97**, 023301, DOI: 10.1063/5.0302424 (2026). https://pubs.aip.org/aip/rsi/article-pdf/doi/10.1063/5.0302424/20886902/023301_1_5.0302424.pdf.
8. Salvadori, M. *et al.* Time-of-flight methodologies with large-area diamond detectors for the effective characterization of tens mev protons. *J. Instrumentation* **17**, C04005, DOI: 10.1088/1748-0221/17/04/C04005 (2022).
9. Pellegrini, G. *et al.* Technology developments and first measurements of Low Gain Avalanche Detectors (LGAD) for high energy physics applications. *Nucl. Instruments Methods Phys. Res. Sect. A: Accel. Spectrometers, Detect. Assoc. Equip.* **765**, 12–16, DOI: https://doi.org/10.1016/j.nima.2014.06.008 (2014). HSTD-9 2013 - Proceedings of the 9th International "Hiroshima" Symposium on Development and Application of Semiconductor Tracking Detectors.
10. Nishizawa, J.-i. P-i-n photodiode. Japanese Patent JP1955-8969A (1955).
11. Villegas, J. *et al.* nlgad gain response to low-penetrating particles. *Nucl. Instruments Methods Phys. Res. Sect. A: Accel. Spectrometers, Detect. Assoc. Equip.* **1072**, 170208, DOI: https://doi.org/10.1016/j.nima.2025.170208 (2025).
12. Carulla, M. *et al.* 50µm thin low gain avalanche detectors (lgad) for timing applications. *Nucl. Instruments Methods Phys. Res. Sect. A: Accel. Spectrometers, Detect. Assoc. Equip.* **924**, 373–379, DOI: https://doi.org/10.1016/j.nima.2018.08.041 (2019). 11th International Hiroshima Symposium on Development and Application of Semiconductor Tracking Detectors.

13. Villegas Dominguez, J. A. *Development of Low Gain Avalanche Detectors (LGAD) for high- and low-penetrating particles in silicon*. Ph.D. thesis, Barcelona, Autonoma U. (2024).

14. Moffat, N. *et al.* Low gain avalanche detectors (lgad) for particle physics and synchrotron applications. *J. Instrumentation* **13**, C03014, DOI: 10.1088/1748-0221/13/03/C03014 (2018).

15. Moffat, N. *Low gain avalanche detectors for particle physics and synchrotron applications*. Ph.D. thesis, University of Glasgow (2020). Ph.D. thesis.

16. Medina, E. *et al.* First experimental validation of silicon-based sensors for monitoring ultra-high dose rate electron beams. *Front. Phys.* **Volume 12 - 2024**, DOI: 10.3389/fphy.2024.1258832 (2024).

17. Kramberger, G. *et al.* Radiation hardness of thin low gain avalanche detectors. *Nucl. Instruments Methods Phys. Res. Sect. A: Accel. Spectrometers, Detect. Assoc. Equip.* **891**, 68–77, DOI: 10.1016/j.nima.2018.02.018 (2018).

18. Borodziuk, S. *et al.* Cavity pressure acceleration: An efficient laser-based method of production of high-velocity macroparticles. *Appl. Phys. Lett.* **95**, 231501, DOI: 10.1063/1.3271693 (2009). https://pubs.aip.org/aip/apl/article-pdf/doi/10.1063/1.3271693/13129058/231501_1_online.pdf.

19. Chodukowski, T. *et al.* High efficiency of laser energy conversion with cavity pressure acceleration. *Sci. Reports* **15**, 21863, DOI: 10.1038/s41598-025-01945-9 (2025).

20. Tchórz, P. *et al.* Proton beams generated via thermonuclear deuterium–deuterium fusion by means of modified cavity pressure acceleration-type targets as a candidate for proton–boron fusion driver. *Phys. Plasmas* **31**, 084503, DOI: 10.1063/5.0207108 (2024).

21. Villegas, J. *et al.* The effects of high-energy carbon co-doping on imb-cnm lgad fabrication and performance. *Sensors* **25**, 5571, DOI: 10.3390/s25175571 (2025).

22. Padilla, R. *et al.* Effect of deep gain layer and carbon infusion on lgad radiation hardness. *J. Instrumentation* **15**, P10003, DOI: 10.1088/1748-0221/15/10/P10003 (2020).

23. Micro-Research Finland. Mrf timing system documentation (2024).

24. Margarone, D. *et al.* In-target proton–boron nuclear fusion using a pw-class laser. *Appl. Sci.* **12**, 1444, DOI: 10.3390/app12031444 (2022).

25. Ziegler, J. F., Biersack, J. P. & Ziegler, M. D. *SRIM, the Stopping and Range of Ions in Matter* (SRIM Company, 2008). 683 pages, available at http://www.srim.org.

26. McNamee, A. *et al.* Contaminant-free alpha particles signature from laser-driven proton-boron fusion plasma using thomson parabola spectrometer. *Laser Part. Beams* **43**, e8, DOI: 10.1017/lpb.2025.10005 (2025).

27. Jakšić, M. *et al.* Ion microbeam studies of charge transport in semiconductor radiation detectors with three-dimensional structures: An example of lgad. *Front. Phys.* **10**, 877577, DOI: 10.3389/fphy.2022.877577 (2022).

28. Manojlovic, M. *Ion Beam Induced Charge (IBIC) Characterization of Low Gain Avalanche Detector (LGAD)*. M.s. thesis, University of Montenegro, Faculty of Natural Sciences and Mathematics, Department of Physics, Montenegro (2022).

29. Laštovička-Medin, G. *et al.* Studies of lgad performance limitations, single event burnout and gain suppression, with femtosecond-laser and ion beams. *Nucl. Instruments Methods Phys. Res. Sect. A: Accel. Spectrometers, Detect. Assoc. Equip.* **1041**, 167388, DOI: https://doi.org/10.1016/j.nima.2022.167388 (2022).

30. Mrkić, D., Laštovička-Medin, G., Manojlović, M., Kramberger, G. & Rebarz, M. Gain suppression in lgad detectors under focused and defocused femtosecond laser beam. *Nucl. Instruments Methods Phys. Res. Sect. A: Accel. Spectrometers, Detect. Assoc. Equip.* **1081**, 170844, DOI: https://doi.org/10.1016/j.nima.2025.170844 (2026).

31. Villegas, J., Kraus, V., Dougados, F., Moll, M. & Hidalgo, S. Gain suppression studies on nlgad detectors. *Nucl. Instruments Methods Phys. Res. Sect. A: Accel. Spectrometers, Detect. Assoc. Equip.* **1083**, 171164, DOI: https://doi.org/10.1016/j.nima.2025.171164 (2026).

32. Jiménez-Ramos, M. C. *et al.* Study of ionization charge density-induced gain suppression in lgads. *Sensors* **22**, 1080, DOI: 10.3390/s22031080 (2022).

33. Manojlović, M. *et al.* Gain response and ion beam-induced donor removal in nlgad detector: Global gain quenching. *IEEE Sensors J.* **25**, 43985–43996, DOI: 10.1109/JSEN.2025.3624206 (2025).

34. Kraus, V. *et al.* Investigating irradiation effects and space charge sign inversion in n-type low gain avalanche detectors. *Nucl. Instruments Methods Phys. Res. Sect. A: Accel. Spectrometers, Detect. Assoc. Equip.* **1080**, 170763, DOI: https://doi.org/10.1016/j.nima.2025.170763 (2025).

35. Wunstorf, R., Bugg, W., Walter, J., Garber, F. & Larson, D. Investigations of donor and acceptor removal and long term annealing in silicon with different boron/phosphorus ratios. *Nucl. Instruments Methods Phys. Res. Sect. A: Accel. Spectrometers, Detect. Assoc. Equip.* **377**, 228–233, DOI: https://doi.org/10.1016/0168-9002(96)00217-3 (1996). Proceedings of the Seventh European Symposium on Semiconductor.

Declaration of generative AI and AI-assisted technologies in the writing process

The authors would like to acknowledge that the AI tool ChatGPT was used to assist in the refinement of language, grammar, and writing style throughout this manuscript. Additionally, ChatGPT was used to generate the graphical abstract. All intellectual content, data, analysis, and conclusions in this article were independently created and verified by the authors.

Author contributions statement

Conceptualization, M.M. and G.L.-M.; methodology, M.M., G.L.-M. and P.T.; experiment administration, T.L., R.L.S. and D.P.; investigation, M.M., G.L.-M., T.L., F.D., N.M. and P.F.-M.; characterization, M.M. and F.D.; writing—original draft preparation, M.M., G.L.-M., P.T. and M.E.; writing—review and editing, M.M., G.L.-M., M.E., P.T., G.K., S.H., E.C. and G.P.; supervision, P.T.; funding acquisition, P.T. All authors have read and agreed to the published version of the manuscript.

Funding

This research was funded by COST Action CA21128 - PROton BOron Nuclear fusion: from energy production to medical applicatiOns (PROBONO). This scientific paper has also been published as part of the international project co-financed by the Polish Ministry of Science and Higher Education within the programe called “PMW”. The research was also funded by the Montenegro Ministry of Education, Science and Innovation through the project “TAIDA: Advancement and Innovation for Detectors at Accelerators” (Contract No. 0402-082/23-1740/5). Support through the María de Maeztu grant CEX2023-001397-M, funded by MICIU/AEI/10.13039/501100011033, is also acknowledged. The work was also supported by Slovenian Agency for Research and Innovation Project J7-4419.

Additional information

Competing interests

The authors declare no competing interests.

Correspondence and requests for materials should be addressed to M.M.